



Numerical investigation of the performance of engineered barriers in controlling stormwater runoff

Alexandros L. Petalas^{a,*}, Aikaterini Tsiampousi^b, Lidija Zdravkovic^b, David M. Potts^b

^a Department of Engineering, Durham University, United Kingdom

^b Department of Civil and Environmental Engineering, Imperial College London, United Kingdom

ARTICLE INFO

Article history:

Received 1 December 2021

Accepted 24 August 2022

Available online 12 September 2022

Editors-in-Chief:

Professor Lyesse Laloui and Professor Tomasz Hueckel

Keywords:

Infiltration modelling
Barrier performance
Runoff

ABSTRACT

In this paper, 2-dimensional, hydro-mechanically coupled finite element analyses are conducted to assess the performance of an engineered barrier, constructed from natural geomaterials, aimed at reducing flood risk in urban environments. The barrier consists of an unsaturated compacted soil layer with water holding properties and a drainage layer of a coarse granular material, that acts as a capillary break, and is constructed on top of the natural soil, in this case London clay. The barrier is vegetated so that its water storage capacity is renewed after each rainfall event. Sophisticated boundary conditions are used to simulate the effect of precipitation and evapotranspiration. The evolution of the rainfall infiltration and runoff rate is simulated both for a treated soil column with an engineered barrier and an untreated one consisting solely of in-situ London Clay. The percolation rate of rainfall water from the bottom of the barrier is also estimated. This comparison highlights the effectiveness of the engineered barrier in reducing the risk of fast flooding, in preventing excessive deformations and in protecting underground infrastructure during wetting and drying cycles. The effect of the hydraulic properties and geometry of the barrier is investigated by means of an extensive parametric analysis. Finally, recommendations for the design of barrier systems are made.

© 2022 The Author(s). Published by Elsevier Ltd. This is an open access article under the CC BY license (<http://creativecommons.org/licenses/by/4.0/>).

1. Introduction

It is widely recognised that urbanisation has caused large changes to the patterns of stormwater flow into or on the ground.¹ Covering land with impervious surfaces, such as roofs, roads and pavements, reduces both the stormwater volume that infiltrates into the soil and the water volume that is transferred from the soil to the air through evapotranspiration. The limited access of the stormwater to the subsurface leads to surface runoff, a phenomenon that occurs when the rainfall rate exceeds the infiltration capacity of the soil during intensive rainfall events.² Excessive runoff water causes flooding, damages critical infrastructure in urban environments and may even lead to loss of human life.³ Moreover, during surface runoff, conventional stormwater drainage systems transfer the polluted water from impervious surfaces to streams, affecting severely their water quality.⁴

Meanwhile, extreme precipitation events that lead to flooding are more common in recent years. Brisbane, Australia (2013), Somerset and Thames Valley, UK (2013–14), Chennai, India (2015), Cumbria, Lancashire and Yorkshire, UK (2015–16), Evia,

Greece (2020) are a few recent examples. The British Environment Agency estimated the economic cost of the 2015 to 2016 winter floods in the UK at £1.6 billion.⁵ Climate projections for the rest of the century show intensification of daily precipitation extremes.⁶ The combination of intense rainfall events and limited access of the water to the ground increase flooding risk significantly. To reduce the impact of these events on urban environments and communities, more efficient drainage systems must be designed, with natural materials and at reduced cost.

The construction and utilisation of Sustainable Drainage Systems (SuDS), constructed with natural resources and materials, tackle this problem in a sustainable manner. The basic principle of the approach involves slowing down and reducing the quantity of surface water runoff from a developed area, to manage downstream flood risk and reduce the risk of runoff driven pollution.⁷ SuDS are utilising permeable surfaces that allow infiltration and storage of stormwater into the ground to mimic natural flow rates and volumes. Moreover, they promote evapotranspiration and support the natural water cycle. They need less energy than conventional drainage systems, mainly due to the reduced use of pumping, and have lower greenhouse emission, due to the natural resources and process that are utilised.

New types of climate adaption control engineered barriers, constructed in urban areas, can provide sufficient drainage capacity, but also protect existing geo-infrastructure from the impacts

* Corresponding author.

E-mail address: alexandros.petalas@durham.ac.uk (A.L. Petalas).

of climate change. To achieve that, the systems must combine: (a) increased infiltration capacity to facilitate the inflow of rainfall water and to reduce runoff; (b) enhanced water holding capacity to efficiently store the rainfall water, provide a healthy environment for vegetation growth and prevent changes in stresses, thus protecting underground infrastructure from excessive displacements; (c) low compressibility to minimise ground deformation; (d) enriched evapotranspiration, to provide a natural drainage path for the rainfall water.

The performance of barriers that are constructed with natural materials is heavily dependent on their hydraulic and mechanical properties at their state after construction (permeability, compressibility, density etc.). Since these materials can be engineered to a very wide range of properties, which cannot realistically be optimised experimentally, a thorough infiltration capacity analysis is needed to identify the key properties that influence the performance of the barrier. A review of rainfall infiltration analysis was recently presented in Ref. 8. Two widely used basic infiltration models are the Green–Ampt⁹ and Richards¹⁰ models. The Green–Ampt model describes the downward movement of a wetting front and can be expressed as an ordinary differential equation, by combining capillary theory and Darcy's law. Various researchers have used the Green–Ampt model as a basis to formulate more advanced analytical and numerical rainfall infiltration models that overcome the limited applicability (single layered, homogeneous and isotropic porous media, etc.) of the original model.^{11–16}

On the other hand, the Richards model combines the continuity equation (conservation of volume) with Darcy's law and leads to a partial differential equation (PDE) that describes flow in unsaturated porous media. Appropriate boundary conditions can be utilised for the modelling of rainfall precipitation and infiltration. Even though there exist analytical solutions for the Richards equation, those are limited to simplified conditions, which do not represent realistically the non-linear hydraulic response of unsaturated soils. A variety of numerical methods (e.g. the Finite Element or Finite Difference methods) have been employed in the literature to solve Richards PDE.^{17–19} However, a common assumption of the simple or more advanced models that are based on the Green–Ampt or Richards equations is that the hydraulic properties, the infiltration capacity and the flow characteristics of a soil are not affected by its mechanical properties and response.

Extensive research has been performed to analyse the performance of capillary evapotranspirative covers for hazardous waste landfills (e.g. Refs. 20–22). Those systems aim to control percolation of rainfall water into the underlying waste,²² and thus, research focused heavily on the analysis of the flow through the barrier^{23–25} using numerical methods that are not taking into account the coupled flow-deformation characteristics, since the settlements of the cover is not a critical design criterion.

In recent years, a good number of works have been presented in the geotechnical engineering literature, focusing on soil–atmosphere interaction and its effect on critical infrastructure. The majority of those works focuses on the stability of man-made and natural slopes, since rainfall induced slope failures and landslides are major geohazards. A review on the numerical methods for slope–vegetation–atmosphere interaction can be found in Ref. 26. The application of hydro-mechanically coupled finite element analysis^{27–31} and finite difference analysis^{32–34} in soil–atmosphere–interaction, has shed light on the mechanisms that lead to stability problems but it has not been widely used for the design and optimisation of climate adaption control barriers, whose performance depends on the interplay between the hydraulic and mechanical properties of the unsaturated compacted geomaterials that are used for their construction.

Developing design protocols for the new generation of climate adaption control technologies is the declared research goal of

the research project CACTUS (Climate Adoption Technologies in Urban Spaces), which encompasses collaboration between 6 UK universities and a number of industrial partners who combine experimental and numerical work to achieve this goal. As part of this effort, the current paper investigates the performance of engineered barriers, by means of advanced hydro-mechanically coupled finite element analysis. The work focuses on the barrier's ability to control surface runoff initiation and excessive percolation to the underlying layers during intense rainfall events. The full process of construction and interaction of the barrier with the atmosphere is simulated. Its performance is compared against a soil profile consisting of natural soil during the same intense rainfall events. The advanced numerical analysis permits extensive parametric analyses, with the purpose of optimising the design and controlling runoff and percolation effectively. This work aims to assist the construction of engineered barriers in real-life projects as well as the experimental testing of full- and small-scale models that will take place as part of the CACTUS research project, by identifying the soil properties which are critical for runoff and percolation control, as well as favourable ranges for their magnitude.

2. Soil–atmosphere interaction finite element analysis

2.1. Overview

The rainfall infiltration into the soil is modelled by means of hydro-mechanically coupled finite element analysis (HM-FEM). The Imperial College Finite Element Program (ICFEP; Refs. 35, 36) is utilised, where the Biot's consolidation theory extended to unsaturated soils has been implemented. The governing equations and their implementation were presented in Ref. 28, with subsequent modifications detailed in Refs. 37, 38. ICFEP adopts a modified Newton–Raphson solution technique, with an error controlled sub-stepping algorithm, to approximate non-linear mechanical and hydraulic response. Non-linearity in the presented numerical simulations emerges due to the assumed non-linear mechanical and hydraulic behaviour of the soil and the applied atmospheric boundary conditions that govern the evolution of pore water pressure and seepage. An outline of ICFEP capabilities in terms of boundary conditions, mechanical, permeability and soil water retention models necessary for the analysis of these problems can be found in Ref. 39.

A 2D axi-symmetric mesh is created, as a column of 8-noded quadrilateral elements (Fig. 1). Each element has 16 displacement and 4 pore fluid pressure degrees of freedom. The mesh represents a 45-m deep soil column. The nodes at the bottom of the soil column are fully fixed ($U_z = U_r = 0$) and no change in pore pressure is allowed ($\Delta p_w = 0$), assuming an interface of the in-situ soil with a permeable bedrock, e.g. Chalk. The nodes at the two vertical boundaries of the column are fixed in the r (radial) direction (U_r), however, they are free in the z (axial) direction, thus the soil can settle. The applied boundary condition in the z -direction is that of zero shear force ($F_z = 0$). The two vertical boundaries are also assumed impermeable ($q_r = 0$), thus flow of water is one-dimensional. Finally, the applied atmospheric boundary conditions are discussed subsequently.

The numerical simulations are performed in three stages. During the first stage, the soil column in Fig. 1a is subjected to long term soil–atmosphere–vegetation interaction analysis (4 years), to establish the stable seasonal PWP profile.³¹ The soil column consists of 3 m of Weathered London Clay (WLC) and 42 m of London Clay (LC), overlaying the Chalk bedrock.

At Stage 2, the top 1 m of the column is excavated and a 1 m deep engineered barrier is constructed in its place. The barrier consists of a 0.2 m deep Drainage Layer (DL) at the

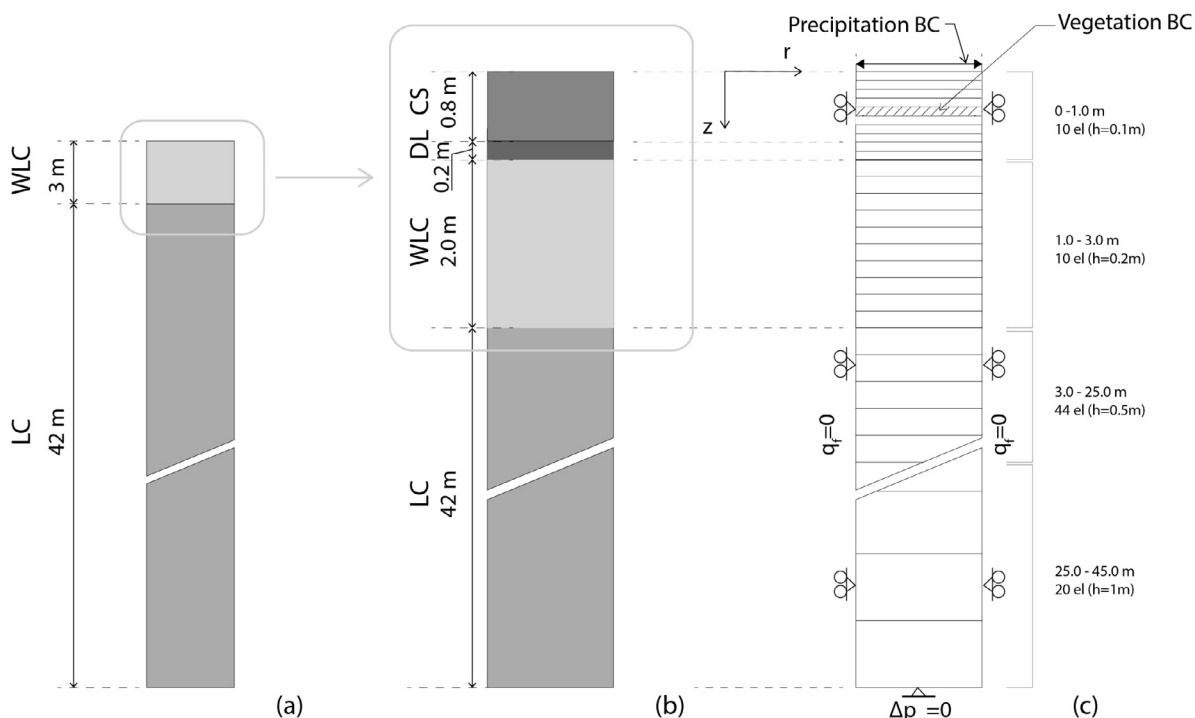


Fig. 1. (a) In-situ soil conditions, Weathered London Clay (WLC), London Clay (LC); (b) Barrier construction, Drainage Layer (DL), Compacted Soil (CS); (c) Finite element mesh and boundary conditions.

base and a 0.8 m thick Compacted Soil layer that reaches the original ground surface (CS; Fig. 1b). An additional year of barrier-atmosphere-vegetation interaction analysis is performed at this stage, to establish the pore water pressure profile within the column, at the commencement of the intense rainfall events. Finally, at Stage 3, rainfall events of different intensity are applied to investigate the performance of the barrier system in controlling water runoff. The time of runoff initiation, the infiltration and runoff rate, and the accumulated runoff water volume are estimated during the rainfall events, and the barrier performance is compared with the untreated soil column, that has been subjected to the same soil-atmosphere-vegetation interaction history and the same rainfall events.

2.2. Precipitation boundary condition

Rainfall is simulated with the precipitation boundary condition (BC) in ICFEP, which has a dual purpose: a flow rate q_n , equal to the rainfall intensity, and a pore water pressure condition, p_{fb} , are prescribed in every increment for which this BC is active. At the beginning of such increments, the algorithm compares the pore water pressure at each of the boundary nodes to p_{fb} ; if found to be more tensile, then the flow rate of q_n is applied (rainfall intensity) and the BC acts as an infiltration BC; otherwise the constant pressure p_{fb} is applied, when ponding and surface runoff occurs. More details about the development and implementation of the precipitation boundary condition in ICFEP can be found in Refs. 28, 29. The precipitation boundary condition in ICFEP has been utilised for the analysis of slope-atmosphere-vegetation interaction in Refs. 30, 31, 39, 40.

The input flow rate q_n in every increment is based on weather simulation data for central London, obtained via the history+database of meteoblue.com. Weather simulation data are suitable for this study, since the evaluation of the barrier performance does not depend on specific in-situ weather conditions of a particular site. The data have a spatial resolution between 4 and 30

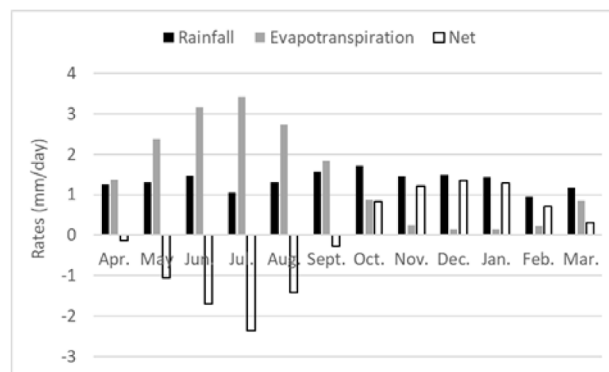


Fig. 2. Precipitation and potential evapotranspiration simulation weather data for London area (source: meteoblue.com).

km, and are complete without data gaps, providing hourly and daily time resolution. The database is extensively validated and verified with recordings from weather stations. Based on the last 10 years (2009–2019), a typical annual precipitation history is derived, by averaging the daily precipitation water volumes for each month of the year. The precipitation data, for the derived typical year in monthly averages, are presented in Fig. 2.

The weather input for the long-term analysis of Stage 1 is in monthly averages. An additional year of barrier-atmosphere-vegetation interaction analysis is performed at Stage 2, before the application of the intense rainfall events. Daily averages of the weather simulation data are used for this additional year, to achieve higher accuracy of the pore fluid pressure profile established at the commencement of the intense rainfall simulation.

2.3. Evapotranspiration boundary condition

Evaporation and transpiration are simulated in a simplified manner, as a combined evapotranspiration outflow source (sink

term) in the continuity equation. This is made possible by applying the vegetation BC presented in Ref. 41. The potential evapotranspiration rate, T_p is an input for each increment of the analysis. Based on a root water uptake model (Fig. 3), the actual rate of water outflow applied as the sink term in the continuity equation is calculated as:

$$S_{acc} = \alpha S_{max} = \frac{2\alpha T_p}{R_{max}} \left(1 - \frac{R}{R_{max}}\right) \quad (1)$$

where S_{max} is the maximum water outflow when water is unlimited, R is the depth within the root zone and R_{max} is the maximum root depth (input); below this depth $S_{max} = 0$. In the analyses presented here $R_{max} = 0.2$ m. The actual outflow rate S_{acc} is calculated by multiplying S_{max} by a suction-dependent parameter α , according to Feddes et al.⁴². The variation of α with suction is illustrated in Fig. 3. Suctions S_1 (anaerobiosis point), S_2 , S_3 and S_4 (wilting point) are input parameters and were taken as 0, 5, 50 and 1500 kPa, respectively.

The fact that S_{acc} depends on suction via α makes the root water uptake model non-linear, as was highlighted in Ref. 41. At the beginning of the increment, S_{acc} is calculated with the current α based on Eq. (1), at the Gauss points of each element within the root zone. The equivalent nodal flow rates are estimated via numerical integration. However, at the end of the increment, α will vary compared to the initial estimation, since the pore water pressure has changed due to the boundary conditions imposed. This leads to out-of-balance nodal flows, which are minimised with an iterative procedure, until convergence is achieved within a prescribed acceptable tolerance.⁴¹ The next increment of the analysis is then performed.

The input potential evapotranspiration rate, T_p , is estimated from the weather simulation data for central London. This estimation is done based on the FAO Penman–Monteith method,⁴³ that calculates the reference evapotranspiration from the daily precipitation data, average temperature, relative humidity, wind speed and shortwave radiation. The calculated potential evapotranspiration, in monthly averages, is given in Fig. 2 and is used in Stage 1. In Stage 2, daily average data are used, calculated by the FAO Penman–Monteith method, consistent with the daily average precipitation data.

2.4. Hydraulic soil properties

The fluid flow through both the unsaturated and saturated soil layers is governed by Darcy's law. For the case of the engineered barrier, consisting of the unsaturated compacted soil layer, in addition to the suction dependent permeability, the soil water retention characteristics are considered via the Soil Water Retention Curve (SWRC).

The hydraulic parameters of London Clay (LC) are well described in the literature and have been employed in previous studies (e.g. Ref. 44). The saturated permeability of LC can be expressed as a function of the mean effective stress as³⁵:

$$k_{sat} = k_0 e^{c_k p'} \quad (2)$$

where c_k is a fitting parameter, and k_0 is the reference isotropic permeability. c_k and k_0 are input parameters for the numerical model.

A variable permeability model, that accounts for the effect of desiccation crack opening (drying) and closing (wetting), is depicted in Fig. 4 and employed for the Weathered London Clay (WLC). The model was introduced in Ref. 45 as:

$$\log k = \log k_{sat} + \frac{\sigma_T - \sigma_{T1}}{\sigma_{T2} - \sigma_{T1}} \log \left(\frac{k_{max}}{k_0} \right) \quad (3)$$

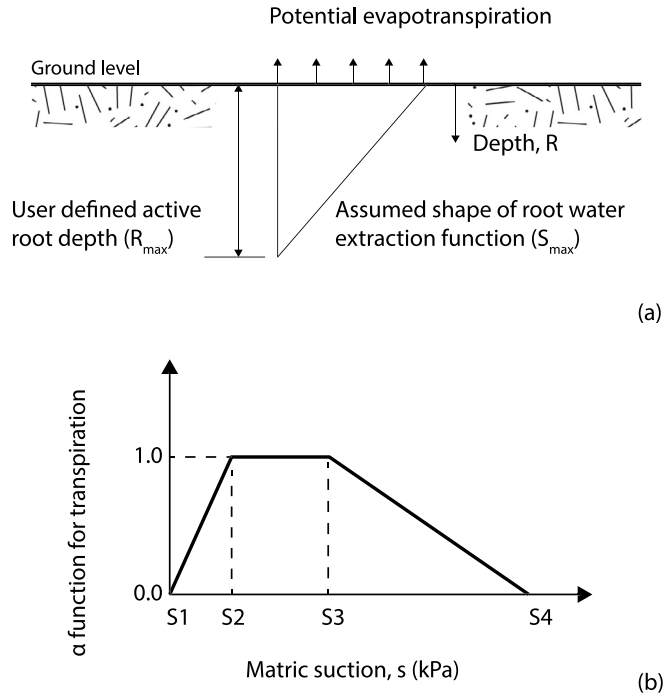


Fig. 3. (a) Water extraction function when $\alpha = 1$; (b) Variation of α function with suction modified from Ref. 41.

where σ_T is the current tensile total principal stress; σ_{T1} and σ_{T2} are two tensile total stress limits, in between which the $\log k$ varies linearly; k_{max} represents the maximum bulk permeability of the cracked ground. The model is able to account for the increased permeability of cracked soil during “dry” months, and the decreased permeability due to crack closure, during “wet” months. The parameters for the variable permeability of unweathered (Eq. (2)) and weathered (Eq. (3)) LC are summarised in Table 1. Both layers are assumed fully saturated.

Finally, the permeability properties and SWRC for the compacted soil (CS) and the drainage layer (DL) of the engineered barrier are defined. The DL is assumed to be constructed with a coarse-grain gravelly sand material. The calibration of its hydraulic properties is based on data for gravelly sand reported in Ref. 46. The CS is assumed to be constructed with a silty clay material, tested in Ref. 47, while the calibration of the unsaturated permeability and SWRC functions in ICPEP were presented in Refs. 48, 49. The CS layers provides the water holding capacity and the DL the capillary break function due to its coarser fraction.

For both layers, the logarithm of the permeability varies linearly with suction, allowing the permeability of intact saturated soil, k_0 to reduce with increasing equivalent suction s_{eq} , until reaching a prescribed minimum value, k_{min} , within the prescribed suction limits s_{eq1} and s_{eq2} . The mathematical expression is given as:

$$\log k = \log k_0 + \frac{s_{eq} - s_{eq1}}{s_{eq2} - s_{eq1}} \log \left(\frac{k_0}{k_{min}} \right) \quad (4)$$

where $s_{eq} = s - s_{air}$ is the current equivalent suction; s is the current value of matric suction; s_{air} is the suction value at air-entry. The resulting permeability curves are presented in Fig. 5. Based on the data and calibration presented in Fig. 5, the permeability of the DL will decrease eight orders of magnitudes during the fast desaturation of this coarse-grain material due to suction increase. This mechanism makes the DL a capillary break layer, since it has the property of stopping the flow when it is under suction.

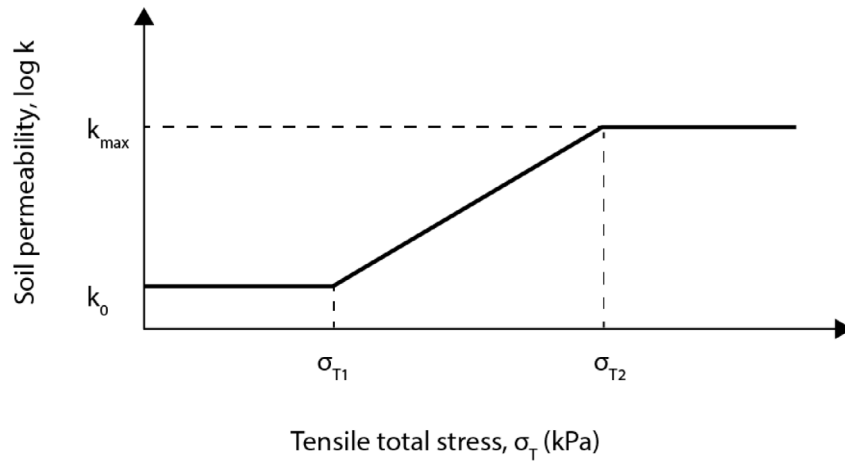


Fig. 4. Assumed variation of soil permeability with major tensile stress due to desiccation cracking.

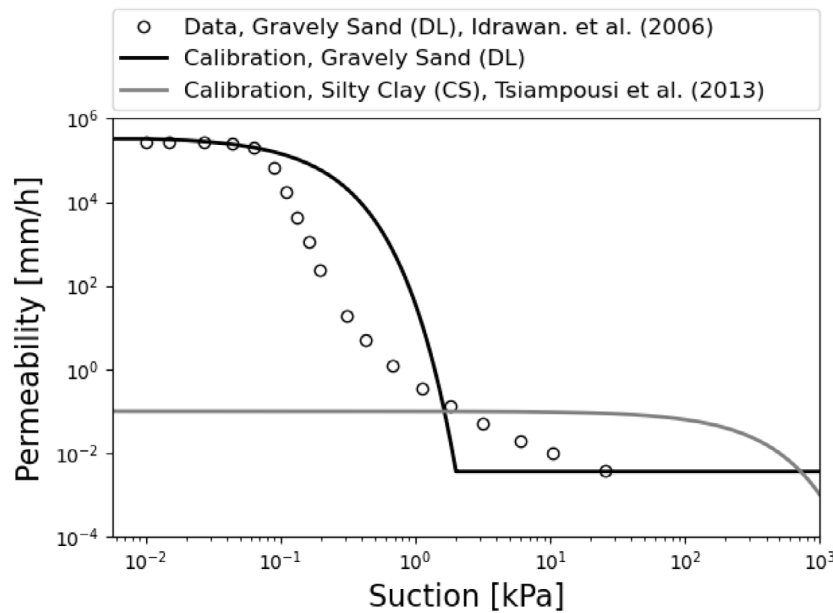


Fig. 5. Assumed variation of soil permeability with suction during desaturation.

The SWRC employed for the silty clay layer⁴⁹ is described as:

$$S_r = \frac{1 - s_{eq}/s_{eq0}}{1 + a_{d,w}s_{eq}} \quad (5)$$

where s_{eq0} is the equivalent suction at zero degree of saturation, S_r ; $a_{d,w}$ is a fitting parameter for the primary drying (d) and wetting (w) curves. By $a_d = a_w$ a non-hysteretic SWRC is considered here.

The SWRC employed for the gravelly sand layer is described as:

$$S_r = \left(\frac{1}{1 + ((s_{eq} - s_{eq,des})a)^n} \right)^m (1 - S_{r,0}) + S_{r,0} \quad (6)$$

where $S_{r,0}$ is the minimum degree of saturation; $s_{eq,des}$ is the suction at the beginning of desaturation and a , n and m are fitting parameters for this non-hysteretic SWRC. Scarfone et al.⁵⁰ showed that SWRC hysteresis may affect the hydraulic performance of a capillary barrier, but is omitted here for simplicity. The resulted SWRC are presented in Fig. 6. The hydraulic input parameters for all layers are summarised in Table 1.

2.5. Mechanical soil properties

The mechanical behaviour of WLC and LC are simulated with the nonlinear elasto-plastic Mohr–Coulomb (MC) constitutive model, with model parameters given in Table 2. The MC model is coupled with the ICG3SM nonlinear elastic small strain overlay model of Taborda et al.⁵¹, for the two materials. The material parameters for the latter model are also summarised in Table 2. The calibration of the MC and small-strain nonlinear elastic models for weathered and unweathered London clay was presented in Ref. 31, while similar values have been employed in Ref. 52. The mechanical behaviour of the DL is simulated with a linear elastic model and its stiffness is independent of suction. Young's modulus and Poisson ratio representative for gravelly sand soils are chosen and their are presented in Table 3.

The mechanical behaviour of CS in the engineered barrier is simulated by a constitutive model detailed in Ref. 48. This is an extended and modified version of the Barcelona Basic Model,⁵³ first implemented in ICFEP by Georgiadis et al.⁵⁴. The model adopts two independent stress variables, the equivalent suction, s_{eq} , as introduced in Eq. (4), and the equivalent stress:

$$\sigma = \sigma_{net} + s_{air} \quad (7)$$

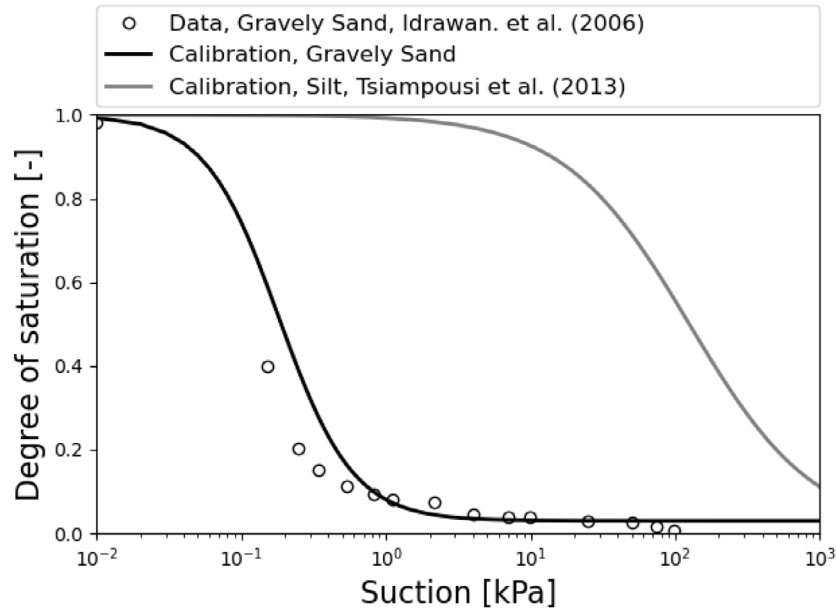


Fig. 6. Assumed soil water retention curves for the materials of the engineered barrier.

Table 1

Soil hydraulic properties of LC, WLC, DL and CS.

Description	Symbol	Value
Permeability London Clay (Eq. (2))		
Isotropic reference permeability	k_0 [mm/h]	1.33E-2
Fitting parameter	c_k [m ² /kN]	0.007
Permeability Weathered London Clay (Eq. (3))		
Isotropic reference permeability	k_0 [mm/h]	1.55E-1
Total principle tensile stress limit	σ_{T1} [kPa]	0
Total principle tensile stress limit	σ_{T2} [kPa]	100
Ratio of max and saturated k	k_{max}/k_0	100
Permeability drainage layer		
Isotropic reference permeability	k_0 [mm/h]	3.6E+5
Equiv. suction limit	s_{eq1} [kPa]	0
Equiv. suction limit	s_{eq2} [kPa]	2
Ratio of min and saturated k	k_0/k_{min}	10E+8
Permeability Compacted soil (Eq. (4))		
Isotropic reference permeability	k_0 [mm/h]	10
Equiv. suction limit	s_{eq1} [kPa]	0
Equiv. suction limit	s_{eq2} [kPa]	1000
Ratio of min and saturated k	k_0/k_{min}	100
SWRC of the drainage layer (Eq. (6))		
Equiv. suction at beginning of saturation	$s_{eq,des}$ [kPa]	0
Degree of saturation at long-term	$S_{r,0}$	0.03
Fitting parameter	a	5.5
Fitting parameter	n	1.7
Fitting parameter	m	1.0
SWRC of the Compacted soil (Eq. (5))		
Suction at air-entry value	s_{air} [kPa]	0
Equiv. suction at zero S_r	s_{eq0} [kPa]	100 000
Fitting parameter (drying)	a_d	0.008
Fitting parameter (wetting)	a_w	0.008

where $\sigma_{net} = \sigma_{total} - u_\alpha \mathbf{I}$, u_α being the air-pressure and \mathbf{I} the second order identity tensor. This formulation allows the transition from saturated to unsaturated states at the air-entry value of suction. Both strength and stiffness of the simulated unsaturated material depend on the equivalent suction s_{eq} , during drying and wetting. Further details on the effect of suction on the strength and stiffness of the soil, using the adopted constitutive law can be

Table 2

Soil mechanical properties of London Clay (LC) and Weathered London Clay (WLC).

London Clay, Weathered LC	
Mohr-Coulomb model	
Symbol	Value
ϕ [°]	23
c [kPa]	7
ν [-]	0.3
ψ [-]	0
Small strain overlay model	
Symbol	Value
G_0 [kPa]	955
K_0 [kPa]	1665
G_{min} [-]	2000
K_{min} [-]	3000
m_G [-]	0.7
m_K [kPa]	0.7
a_0 [-]	1.81E-4
$R_{G,min}$ [-]	5E-2
$R_{K,min}$ [-]	7.9E-2
r_0 [-]	3E-4
s_0 [-]	1.1

Table 3

Soil mechanical properties of Drainage Layer (DL).

Drainage Layer (DL)	
Linear elastic	
Symbol	Value
E [kPa]	180 000
ν [-]	0.2

found in Refs. 48, 54. The mechanical material properties in this work are the same as those employed in Ref. 40 and are summarised in Table 4, corresponding to an unsaturated compacted silty soil tested by Estabragh and Javadi⁴⁷. The over-consolidation ratio is used to initialise the hardening parameter p_0^* of the yield surface and is set to 3.5 for the compacted soil after the barrier construction.

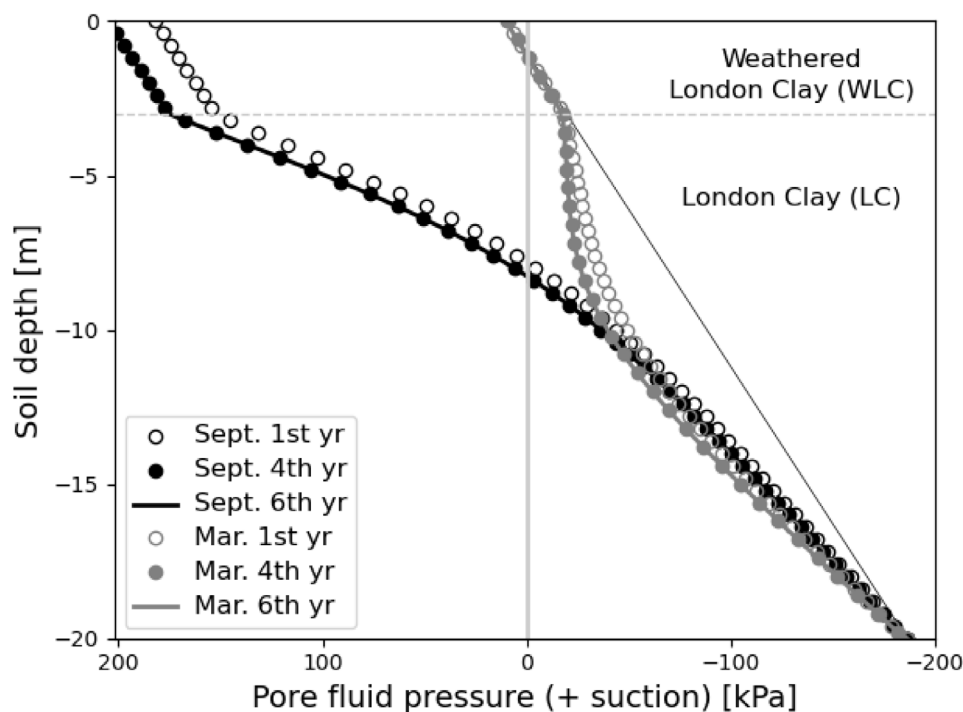


Fig. 7. Pore water pressure profile during the long duration analyses of Stage 1, for a “dry” and “wet” month.

Table 4

Soil mechanical properties of the compacted unsaturated soil (CS).

Compacted unsaturated soil			
Georgiadis et al. ⁵⁴ model			
Symbol	Value	Symbol	Value
α_g, α_f [-]	0.7	$\lambda(0)$	0.086
μ_g, μ_f [-]	0.9999	κ	.005
M_g, M_f [-]	0.899	ν_1	2.12
α_{HV} [-]	0.6	p^c	1
n [-]	0.5	r	0.06
β_{HV} [kPa]	0.25	β	0.001
m [-]	0.5	λ_s	0.3
s_{air} [kPa]	0.0	κ_s	0.08
s_0 [kPa]	1000	p_{atm} [kPa]	100
K_{min} [-]	300		
G/p_0 [-]	15		

3. Numerical simulations

3.1. Seasonal pore fluid pressure profile initialisation (Stage 1)

At the beginning of the analysis, soil stresses are initialised based on the unit weight of London Clay (LC), i.e. 19.1 kN/m^3 , above and below the ground water table (GWT). The coefficient of earth pressure at rest, K_0 , is 2.1 at the ground surface, reducing to 0.6 at 15 m below the ground surface, linearly. The GWT is 1-m deep and the pore water pressure profile is hydrostatic, with suction developing above the GWT.

In Stage 1, a long duration analysis was performed to compute the stabilised seasonal pore water pressure (PWP) in the soil profile, with the assigned hydraulic and mechanical properties discussed in Sections 2.4 and 2.5, respectively. The climatic input data are those discussed in Sections 2.2 and 2.3. Fig. 7 presents the resulting PWP profiles in the top 20 m of the 45 m deep soil column. It is concluded that 4 years annual cycles are sufficient to achieve the representative stabilised PWP profile for this set of soil properties, as the filled circular points (4 years) are shown to

coincide with the solid lines (6 years). This result is consistent for September, when the monthly average evapotranspiration rate is higher than the precipitation rate, and for March when the opposite holds.

It is of interest to note a different trend in the PWP profiles in the WLC compared to the LC. More specifically, the PWP profile follows a non-linear distribution with depth in LC, whereas, the distribution is linear in WLC. This is attributed to the differences in the reference and evolving permeability. The reference permeability, k_0 , of the WLC is $1.55\text{E}-1 \text{ mm/h}$, approximately one order of magnitude higher than the reference permeability of LC ($1.35\text{E}-2 \text{ mm/h}$).

3.2. Excavation of in-situ soil and construction of the barrier system (Stage 2)

At Stage 2, the engineered soil barrier is constructed, by applying the excavation and construction boundary conditions described in Ref. 35. The elements of the top 1 m of the soil column in Fig. 1a are removed and the same elements are constructed again, but with the properties of the Drainage Layer (DL) and Compacted Soil (CS) and become again a part of the active mesh.³⁵ The process occurs in 4 time steps, of $\Delta t = 1 \text{ day}$, each. The initial suction in the CS upon construction is an input in the analysis and 50 kPa was assumed, while 8 kPa was assumed in the DL. The suction profile within the barrier depends both on the type of soil and the compaction effort during construction. Since data for a site specific constructed barrier are not available, a low suction value is assumed for the coarse-grained gravelly sand and a higher suction value for the fine silty-clay. A degree of saturation consistent with the SWRC (Eqs. (5) and (6)) was also input. The case where the soil column contains the engineered barrier is abbreviated as the “treated soil column”, while the case with the in-situ soil is called the “untreated soil column”, in the following text for clarity.

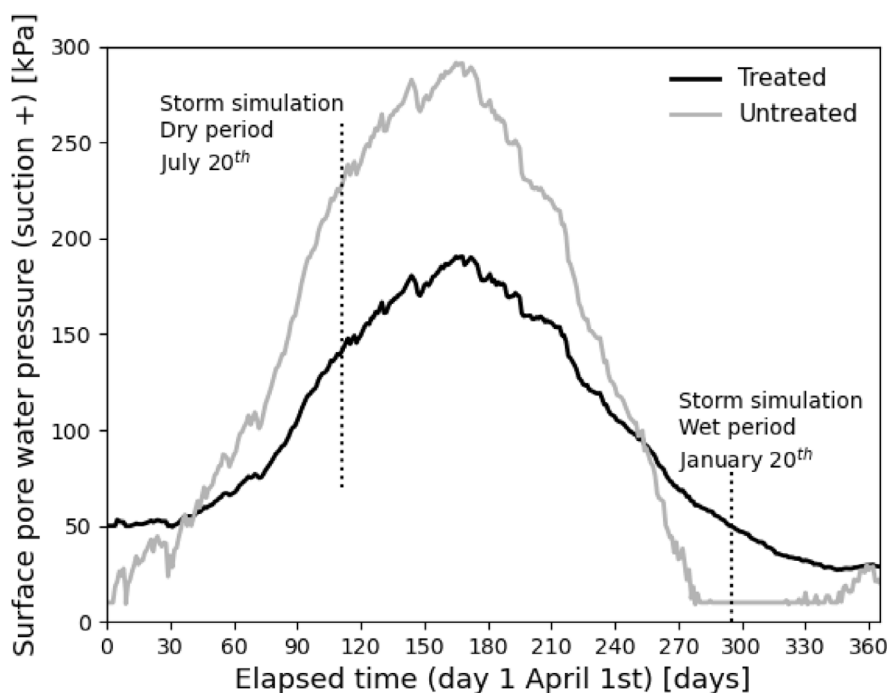


Fig. 8. Surface pore water pressure prediction, during one year of soil–atmosphere–vegetation interaction.

One additional year of barrier–atmosphere–vegetation interaction, with daily average precipitation and evapotranspiration data, is performed at Stage 2. This simulation provides a more detailed description of the suction variation within every day of the year since the monthly averaging process smooths out some critical maxima and minima in the resulting annual evolution of suction. Each increment of the analysis represents 1 day, and thus 365 increments are applied.

The calculated water pressure (suction positive), at a node of the top boundary of the soil column, is plotted against time in Fig. 8. The black line represents the treated soil column, while the grey line represents the untreated case. Day number 1 in Fig. 8 is April 1st. The initial suction (day 0) is 50 kPa for the treated case, due to the construction of the compacted soil of the barrier, while in the untreated case it is 10 kPa. This value results from the preceding precipitation-dominant “wet” period at the end of which the precipitation boundary condition switched from a prescribed infiltration rate, equal to the rainfall intensity, to a constant pore pressure of 10 kPa at the same boundary. In both cases, the surface suction has the tendency to increase during the “dry” period of about 6 months, up until day 175, corresponding approximately to the end of September. During this period, the evapotranspiration rates are, on average, higher than the precipitation rates (Fig. 2). The rate of suction increase is higher for the untreated case, hence higher surface suctions are predicted during the “dry” period for the case of the untreated soil, approximately after one month. During the “wet” period (after the initial 6 months), when precipitation rates are higher than potential evapotranspiration rates, the surface suction progressively decreases for both cases. The rate of decrease is higher in the untreated case and the surface suction eventually reaches the 10 kPa constant boundary pore pressure, imposed by the precipitation BC when precipitation is dominant.

Finally, the surface settlement that is developed within the extra year of soil–atmosphere–vegetation interaction is plotted in Fig. 9 for the two cases. It is observed that the construction of the barrier reduces the maximum settlement of the soil column by approximately 50%.

3.3. Barrier performance during intense rainfall (Stage 3)

Rainfall infiltration during intense precipitation events is simulated in Stage 3 during both “dry” and “wet” periods, corresponding to July 20th and January 20th, respectively, as annotated in Fig. 8.

3.3.1. Rainfall simulation during the “dry” period

Fig. 10 compares of the performance of the treated soil column for intense rainfall events in the “dry” period. In Fig. 10 a, b and c, the evolution of surface suction with time is plotted during the 300 min of the $q = 9$ mm/h, the $q = 15$ mm/h and the $q = 18$ mm/h event, respectively. The return periods of the $q = 9$ mm/h, the $q = 15$ mm/h and $q = 18$ mm/h events are $T = 2$ years, $T = 10$ years and $T = 25$ years for the London area, respectively. Runoff is initiated when the surface suction becomes zero and the precipitation BC switches from infiltration rate application to constant pore fluid pressure application, in this case 0 kPa (instead of 10 kPa as in Stage 2). This reflects the assumption that ponding of the rainfall runoff water is not allowed on the soil surface. The bottom percolation rate, i.e., the rate that the water passes through the drainage layer to the soil under the barrier is also calculated. A calculation at the same depth is made for the untreated column too for comparison. It can be seen that the construction of the engineered barrier in the treated soil column (black solid lines) prevents runoff initiation as surface suction is retained in all three cases. Conversely, in the untreated soil column (grey solid lines) runoff occurs for all three cases when the surface suction reaches zero. The rate of the decreasing surface suction increases significantly with increasing rainfall intensity q , in the untreated soil column case (slope of the grey solid line in Fig. 10a, b and c), whereas it is less affected in the case of the treated column. The higher infiltration capacity of the barrier, due to higher permeability and water retention properties, makes it less sensitive to increased rainfall intensity. This will be discussed further later in the paper, through a parametric analysis of the hydraulic properties of the barrier.

Fig. 10 d, e and f, illustrate the infiltration (full squares), runoff (empty square) and bottom percolation (cross-mark) rates, for the

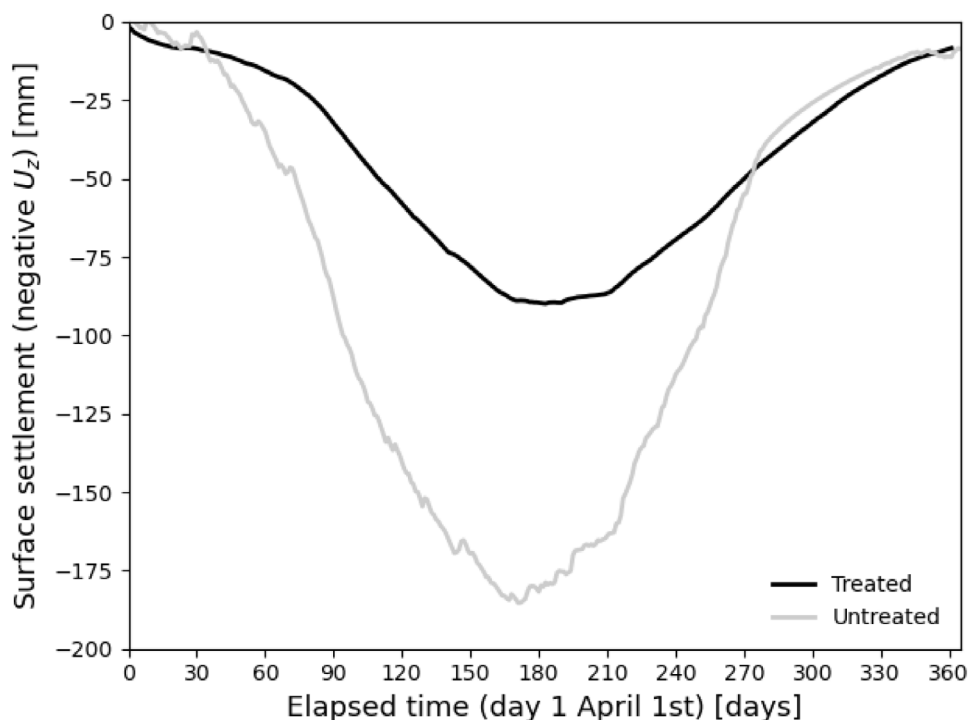


Fig. 9. Surface settlement prediction, during one year of soil-atmosphere-vegetation interaction.

treated (black lines) and untreated (grey lines) cases, during the same intensity rainfall events. In the treated soil column case, the infiltration rate equals the applied rainfall rate for the whole duration 300 min of the rainfall event. The infiltration capacity of the barrier is not exceeded, and the runoff rate remains zero. On the other hand, in the untreated soil column, the infiltration rate equals the rainfall rate up until runoff initiation. After that, it progressively decreases while runoff rate progressively increases. The increasing runoff rate leads to an increase of accumulated runoff as presented in Fig. 10g, h and i. The highest rainfall intensity (Fig. 10c, f and i) leads to the largest accumulated runoff in the untreated case, both because the runoff is initiated sooner, but also because the runoff rate is higher than in the other two cases. The bottom percolation rate is zero for the treated case in all three events. This means that no rainfall water passes through the DL towards the soil layers underneath. The DL acts as a capillary break layer, since its suction remains significantly higher (96 kPa in the middle of the DL) than the value required for the permeability to increase from its minimum desaturated value, according to the unsaturated permeability calibration presented in Fig. 5. In contrast, the rainfall water percolation at equivalent depth to the layers underneath is significant for the untreated case (grey dotted lines with cross-mark).

It can be therefore concluded that the engineered barrier, consisting of the Compacted Soil (CS) and a Drainage Layer (DL) that acts as a capillary break layer, is an efficient solution for controlling runoff and percolation of rainfall water in the layers underneath, during the “dry” period.

3.3.2. Rainfall simulation during the “wet” period

The same three rainfall events introduced above are applied again, but starting during a day of the “wet” period. Fig. 11 a, b and c show that the initial surface suction, at the commencement of the rainfall events ($t = 0$ min), is significantly lower than in the “dry” period (see also Fig. 8). Due to this, the runoff initiation in the untreated case starts within a few minutes after the commencement of each of the three events (grey solid line reaches

zero), while in the treated case even the smaller magnitude of the initial suction is beneficial for preventing runoff even for the extreme case of $q = 18$ mm/h (Fig. 11c). Another critical feature of the untreated soil column’s performance is the high runoff rates after runoff initiation. Fig. 11 d, e and f show that in the case of the untreated soil column the runoff rates reach very quickly their maximum value, which equals the applied rainfall rate. At the same time the infiltration capacity of the column drops to zero. This leads to very large accumulated runoff, as presented in Fig. 11g, h and i. The percolation of rainfall water from the DL to the layers underneath the barrier is zero for all three events in the treated case. Significant suctions are sustained (26 kPa at the end of the most severe 18 mm/h event) in the DL and thus the desaturated permeability remains very low (see Fig. 5). In the untreated case, the percolation of rainfall water at an equivalent with the end of the barrier depth to the layers underneath is zero due to the fact that surface run-off initiates immediately, thus, rainfall water stays outside the soil column.

Finally, the predicted surface heave during the $q = 15$ mm/h intensity, $T = 10$ y return period rainfall events, starting during the “wet” and “dry” periods, is plotted in Fig. 12. It can be seen that the engineered barrier significantly reduces the large surface heave that is observed in the untreated soil column (grey dashed line) during the intense rainfall event of the “dry” period.

From the advanced hydro-mechanically coupled FEM analyses, it is concluded that the construction of the engineered barrier can effectively control the runoff initiation and runoff volume for intense events starting both during the “dry” and the “wet” period. At the same time it minimises the rainfall percolation through the drainage layer to the layers underneath. Additionally, the barrier can potentially control the excess deformation in the top layers during the soil-atmosphere-vegetation interaction throughout the year and leads to significantly reduced heave compared to the untreated case, during an intense event that occurs during summer. These are promising results towards the development of design guidelines for climate adaption solutions for urban environments, that will both reduce the risk from fast flooding and protect shallow underground infrastructure from excessive deformation.

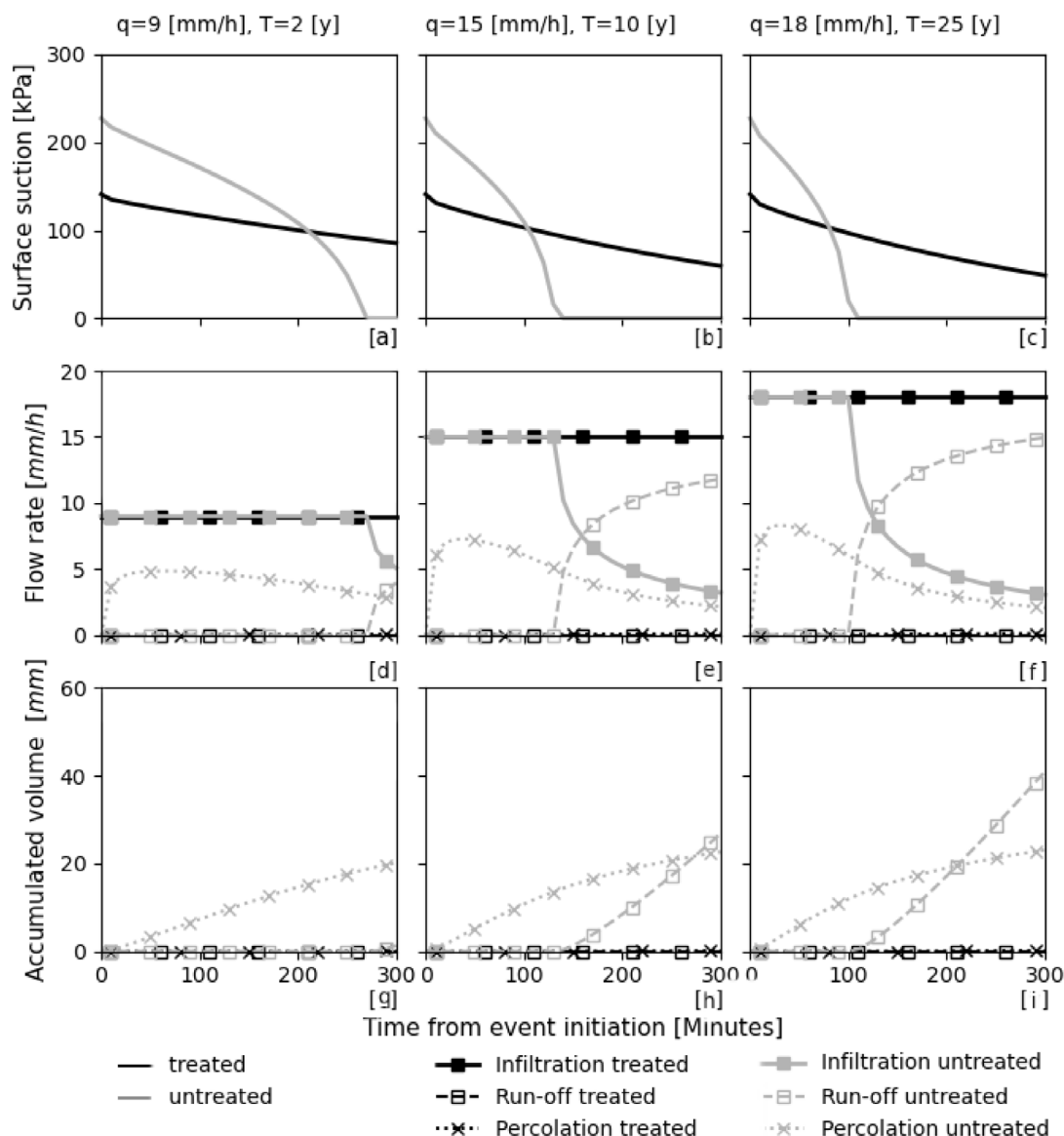


Fig. 10. Performance of the engineered barrier (treated soil column) versus in-situ soil (untreated soil column) during the “dry” period.

3.3.3. Parametric study

The effect of hydraulic properties and depth of the CS layer on the performance of the barrier is examined next by means of a parametric study. Three sets of numerical simulations are summarised in Table 5, where bold values represent variations to reference values adopted in the above base study. A reference value is modified in both the simulation of Stage 2, when the barrier is constructed, and Stage 3, when the intense rainfall event ($q = 15 \text{ mm/h}$) is applied. Since this parametric study focuses on the effect of the hydraulic properties and the depth of the engineered barrier, the modified parameters do not influence the results of Stage 1 (before the barrier’s construction). Finally, the $q = 15 \text{ mm/h}$ is applied during the “wet” period, on the 20th of January as annotated in Fig. 8.

Fig. 13 shows the effect of the reference saturated permeability k_0 of the CS layer (Set 1) on the runoff initiation, runoff rate and accumulated volume, percolation rate and percolation volume, while keeping all the other hydraulic and mechanical parameters the same as detailed in Tables 1, 2 and 4. The runoff initiation is prevented in the two cases where $k_0 = 100 \text{ mm/h}$ and $k_0 = 10 \text{ mm/h}$ (their lines are overlapping in Fig. 13b),

Table 5

Numerical simulation program for parametric study.

	Permeability, k_0 [mm/h]	SWRC, α_d	Depth, D [m]
Set 1	100	0.008	0.8
	10		
	1		
	0.1		
Set 2	10	0.015	0.8
		0.008	
		0.004	
Set 3	10	0.008	0.8
			0.3

whereas runoff initiation is observed for $k_0 = 1 \text{ mm/h}$ and $k_0 = 0.1 \text{ mm/h}$. In the latter case, the runoff is initiated after a few minutes and leads to significant runoff rates and accumulated runoff. In all cases the percolation rate and volume remains zero.

Fig. 14 shows the effect of the SWRC on the performance of the barrier, by testing three different SWRCs that are presented in Fig. 15 and Table 5, keeping the base reference permeability

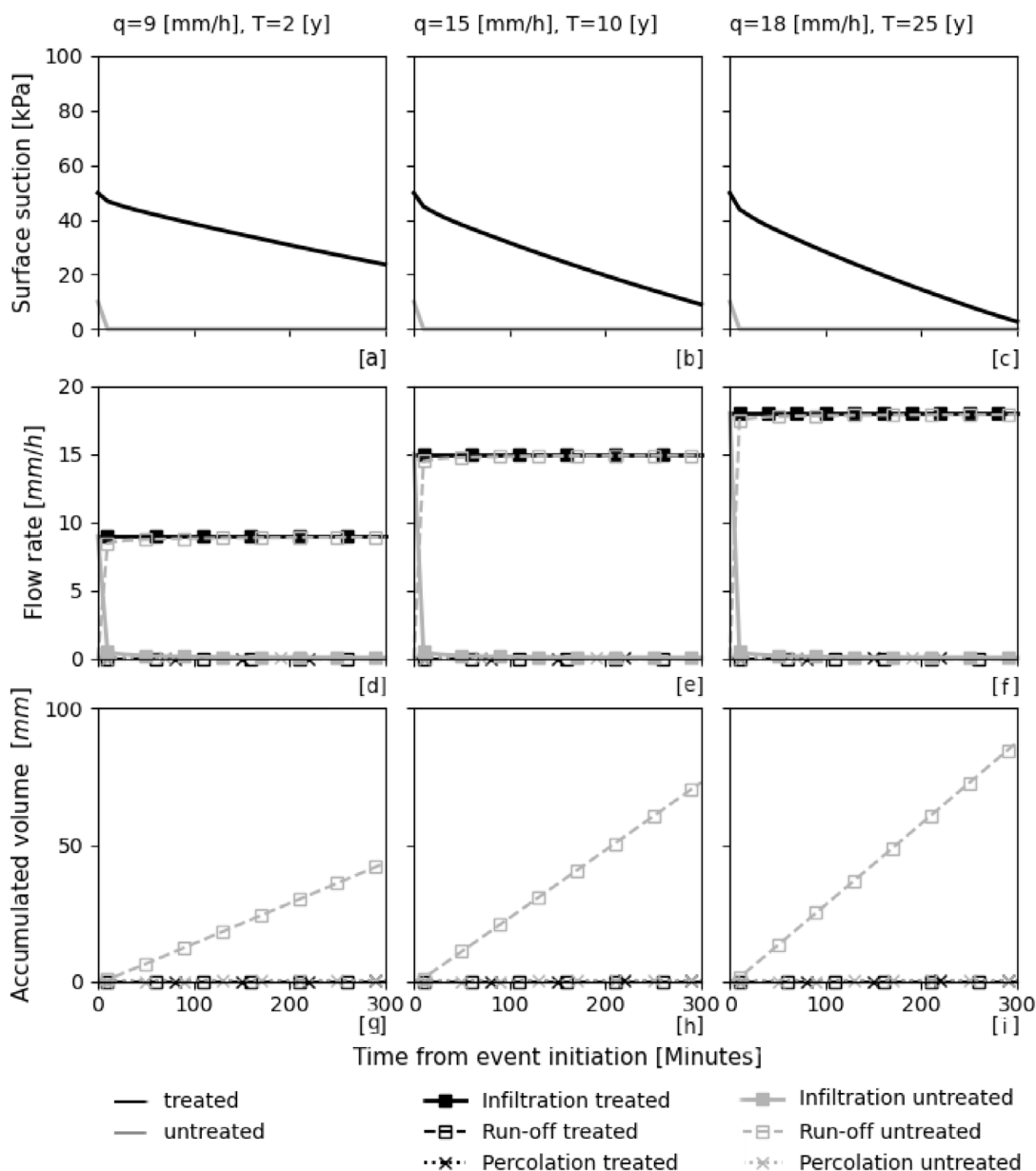


Fig. 11. Performance of the engineered barrier (treated soil column) versus in-situ soil (untreated soil column) during the “wet” period.

the same ($k_0 = 10 \text{ mm/h}$). For the case where $\alpha_d = 0.004$, the initial suction at the commencement of the rainfall simulation is 43 kPa, and the corresponding degree of saturation is 0.88. For the case where $\alpha_d = 0.008$, the initial suction is 53 kPa, and the corresponding degree of saturation 0.84, while for $\alpha_d = 0.015$, the initial suction is 54 kPa and the degree of saturation 0.60. Fig. 14a shows that for the SWRC that sustains higher degree of saturation at a given value of suction (see dotted line with $a_d = 0.004$ in Fig. 15), the infiltration capacity decreases significantly, and runoff is initiated (grey line in Fig. 14 a, b and c). Moreover, the runoff rate increases quickly and leads to significant accumulated runoff. In all cases the percolation rate and volume remains zero.

Finally, the depth of the engineered barrier is examined, since it is a critical design parameter that significantly effects the cost of the construction process. Fig. 16a shows that the reduced depth of the engineered barrier ($D = 0.3 \text{ m}$) lead to runoff, while the $D = 0.8 \text{ m}$ barrier prevents it. It is further observed that the runoff rate increases instantaneously after the initiation (Fig. 16b)

to the maximum rate that equals the rainfall intensity, which is attributed to the fact that the decreased depth barriers get saturated faster.

4. Discussion

From the results of the base and the parametric studies, it is tempting to conclude that a coarse granular geomaterial like sand or gravel is the best candidate for an engineered barrier constructed with the goal of runoff control. The larger permeability and the faster desaturation lead to an enhanced infiltration capacity, thus an improved capability to facilitate intense precipitation events, compared to in-situ fine grained soils. However, a coarse geomaterial reduces the water holding capacity of the barrier, so the water that this system collects tends to flow easier to the underlying layers, causing larger changes in stresses in deeper layers. Moreover, water holding capacity is essential for the healthy growing of vegetation, that can provide a natural drainage mechanism through transpiration.

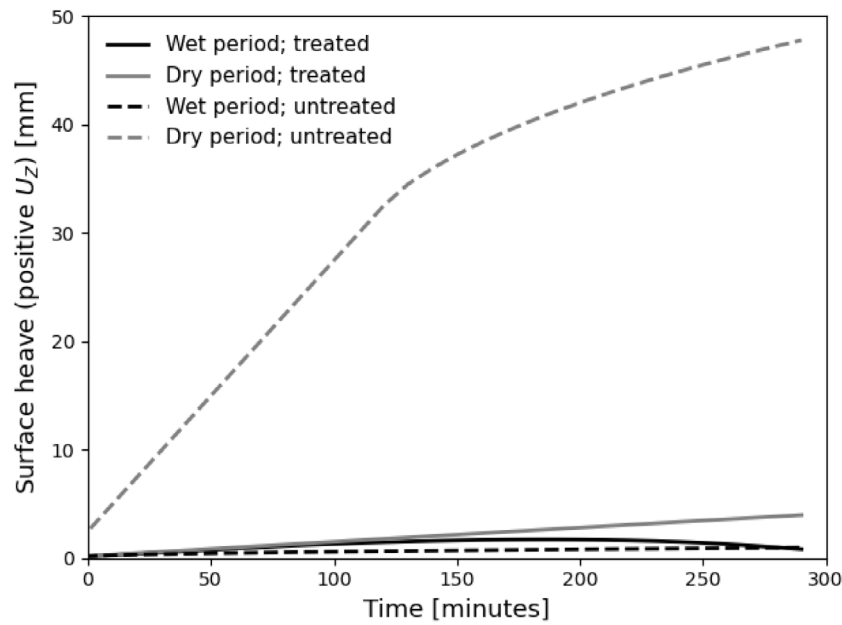


Fig. 12. Surface heave, during the 300 min, $q = 15$ [mm/h] intensity, $T = 10$ [y] return period rainfall events, starting during the wet and dry period.

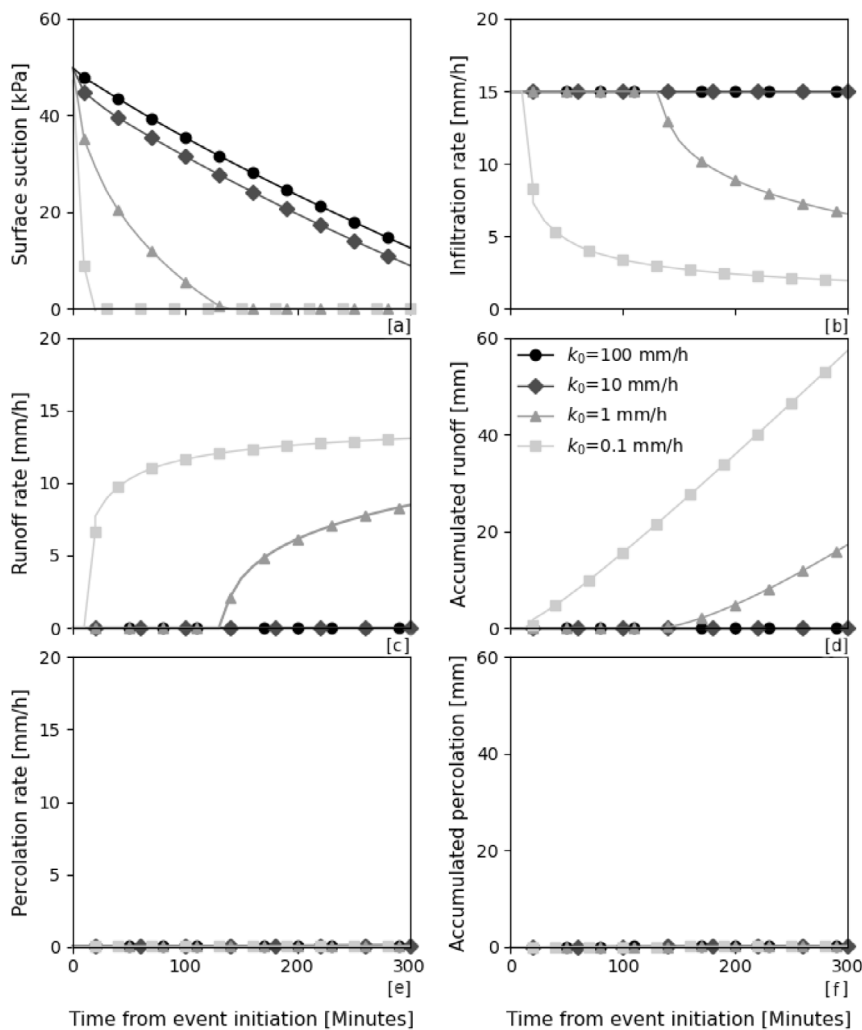


Fig. 13. Effect of reference saturated permeability on the performance of the engineered barrier.

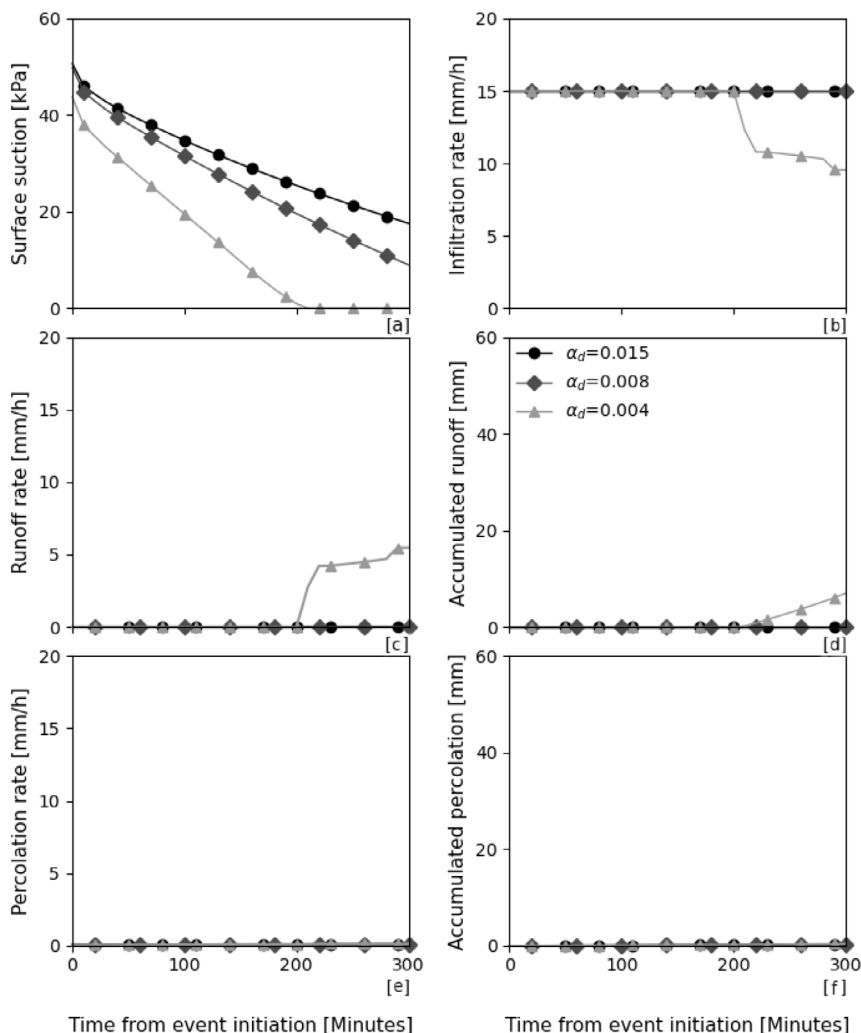


Fig. 14. Effect of the SWRC on the performance of the engineered barrier.

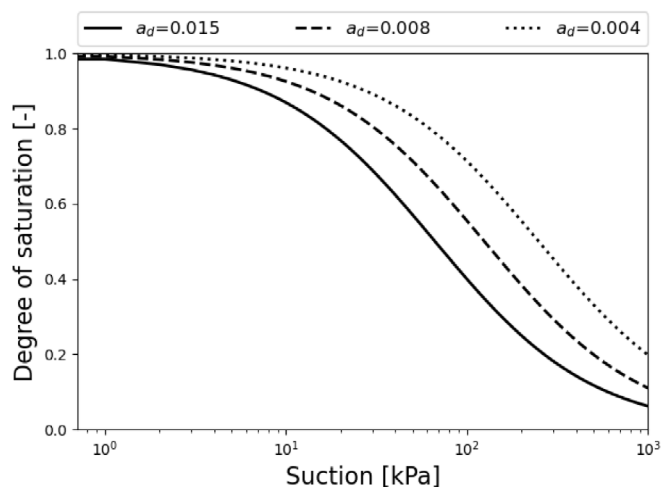


Fig. 15. Soil water retention properties of the engineered barrier.

An optimum balance between the hydraulic properties that increase infiltration capacity, water holding capacity to keep the system functional and compressibility for the system to protect shallow underground infrastructure is thus required. This work

provides a workflow for the analysis of this complicated synergy, by considering all the mechanisms that contribute to the complex hydro-mechanically coupled response.

5. Conclusions

The performance of an engineered barrier in preventing and reducing runoff is investigated in this work, by means of advanced hydro-mechanically coupled FE analyses. The work is mainly focused on the barrier's ability to control runoff initiation and accumulated runoff volumes during intense rainfall events, using the ground and weather conditions associated with the London area, as an example of an urban environment. The main observations from the study can be summarised as follows:

- A compacted unsaturated barrier with increased permeability and water retention properties, compared to those of the in-situ soil, is capable of preventing runoff initiation for intense rainfall events of up to 25 years return period, which may occur in both dry and wet periods of the year.
- The coarse-grained material in the drainage layer acts successfully as a capillary break layer and prevents the percolation of rainfall water to the layers underneath due to the low unsaturated permeability when is under suction. This property makes the barrier successful in protecting underlying underground structures from stress change and excessive deformation.

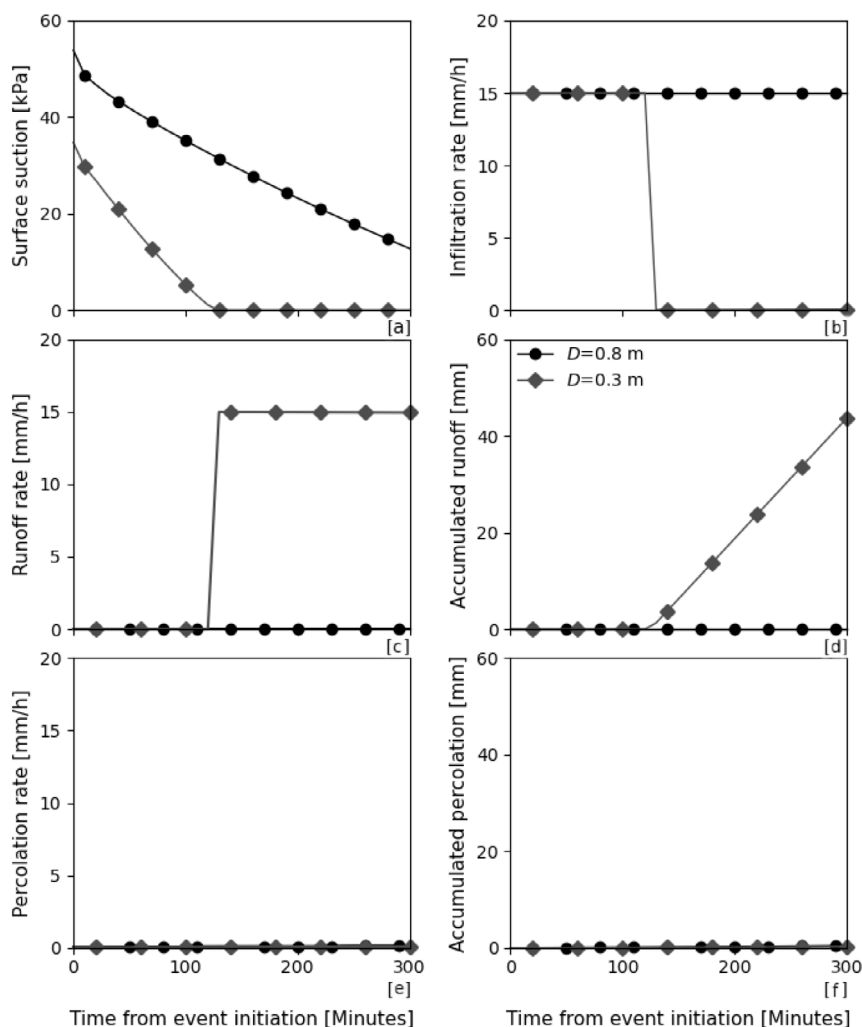


Fig. 16. Effect of the barrier depth on the performance of the engineered barrier.

- The key controlling parameters identified for barrier design are permeability, water retention properties and depth of the barrier.
- It is demonstrated that the permeability of the barrier upon construction needs to be approximately the same as the design rainfall intensity, for the effective runoff control to be achieved.
- It is further shown that the water retention behaviour of the barrier needs to ensure an appropriate lower degree of saturation for the design value of suction, to enable sufficient infiltration capacity and runoff prevention.
- It is finally established that the depth of the barrier needs to be substantial to enable an effective annual balance of water that would ensure that it remains unsaturated. Relatively thin barriers are shown to suffer from rapid saturation during an intense rainfall, thus losing the ability to prevent or control runoff.

CRediT authorship contribution statement

Alexandros L. Petalas: Conceptualization, Methodology, Formal analysis, Visualisation, Writing – original draft. **Aikaterini Tsiampousi:** Conceptualization, Methodology, Supervision, Writing – review & editing. **Lidija Zdravkovic:** Supervision, Writing – review & editing. **David M. Potts:** Supervision, Writing – review & editing.

Declaration of competing interest

The authors declare that they have no known competing financial interests or personal relationships that could have appeared to influence the work reported in this paper.

Acknowledgements

The research leading to these results has received funding from EPSRC, United Kingdom, under the EP/R005834/1 grant, of the project Climate Adaptation Control Technologies for Urban Spaces (CACTUS). All authors approved the version of the manuscript to be published.

References

1. Leopold L. *Hydrology for Urban Land Planning - A Guidebook on the Hydrologic Effects of Urban Land Use*. Technical Report; 1968 URL <http://enviro.lclark.edu/resources/Tryon/Water/Hydrology.pdf>.
2. Mein RG, Larson CL. Modeling the infiltration component of the rainfall-runoff process. 1971:72. URL <http://books.google.com.mx/books?id=3454GQAACAAJ>.
3. Jonkman SN. Global perspectives on loss of human life caused by floods. *Nat Hazards*. 2005;34(2):151–175. <http://dx.doi.org/10.1007/s11069-004-8891-3>.
4. Walsh CJ, Fletcher TD, Ladson AR. Retention capacity: A metric to link system ecology and storm-water management. *J Hydrol Eng*. 2009;14(4):399–406. [http://dx.doi.org/10.1061/\(ASCE\)1084-0699\(2009\)14:4\(399\)](http://dx.doi.org/10.1061/(ASCE)1084-0699(2009)14:4(399)).

5. *Estimating the Economic Costs of the 2015 to 2016 Winter Floods*. Technical Report January; Bristol, UK: Environment Agency; 2018:1–50. URL www.gov.uk/environment-agency.
6. Donat MG, Lowry AL, Alexander LV, O’Gorman PA, Maher N. More extreme precipitation in the world’s dry and wet regions. *Nature Clim Change*. 2016;6(5):508–513. <http://dx.doi.org/10.1038/nclimate2941>.
7. CIRIA. *The SuDS Manual (C753)*. Technical Report; Department for Environmental Food & Rural Affairs; 2015.
8. Morbidelli R, Corradini C, Saltalippi C, Flammini A, Dari J, Govindaraju RS. Rainfall infiltration modeling: A review. *Water (Switzerland)*. 2018;10(12). <http://dx.doi.org/10.3390/w10121873>.
9. Green WH, Ampt GA. Studies on soil physics. Part i. *J Agric Sci*. 1911;4:1–24.
10. Richards LA. Capillary conduction of liquids through porous mediums. *Physics*. 1931;1(5):318–333. <http://dx.doi.org/10.1063/1.1745010>.
11. Corradini C, Morbidelli R, Flammini A, Govindaraju RS. A parameterized model for local infiltration in two-layered soils with a more permeable upper layer. *J Hydrol*. 2011;396(3–4):221–232. <http://dx.doi.org/10.1016/j.jhydrol.2010.11.010>.
12. Corradini C, Flammini A, Morbidelli R, Govindaraju RS. A conceptual model for infiltration in two-layered soils with a more permeable upper layer: From local to field scale. *J Hydrol*. 2011;410(1–2):62–72. <http://dx.doi.org/10.1016/j.jhydrol.2011.09.005>.
13. Deng P, Zhu J. Analysis of effective green-ampt hydraulic parameters for vertically layered soils. *J Hydrol*. 2016;538:705–712. <http://dx.doi.org/10.1016/j.jhydrol.2016.04.059>.
14. Hsu SY, Huang V, Woo Park S, Hilpert M. Water infiltration into prewetted porous media: Dynamic capillary pressure and green-ampt modeling. *Adv Water Resour*. 2017;106:60–67. <http://dx.doi.org/10.1016/j.advwatres.2017.02.017>.
15. Nie WB, Li YB, Fei LJ, Ma XY. Approximate explicit solution to the green-ampt infiltration model for estimating wetting front depth. *Water*. 2017;9(809). <http://dx.doi.org/10.3390/w9080609>.
16. Tan J, Song H, Zhang H, Zhu Q, Xing Y, Zhang J. Numerical investigation on infiltration and runoff in unsaturated soils with unsteady rainfall intensity. *Water*. 2018;10(914):2–16. <http://dx.doi.org/10.3390/w10070914>.
17. Lam L, Fredlund DG. Saturated-unsaturated transient finite element seepage model for geotechnical engineering. *Adv Water Resour*. 1984;7:132–136.
18. Clement TP, Wise WR, Molz FJ. A physically based, two-dimensional, finite-difference algorithm for modeling variably saturated flow. *J Hydrol*. 1994;161(1–4):71–90. [http://dx.doi.org/10.1016/0022-1694\(94\)90121-X](http://dx.doi.org/10.1016/0022-1694(94)90121-X).
19. Belfort B, Younes A, Fahs M, Lehmann F. On equivalent hydraulic conductivity for oscillation-free solutions of richard’s equation. *J Hydrol*. 2013;505:202–217. <http://dx.doi.org/10.1016/j.jhydrol.2013.09.047>.
20. Zornberg JG, LaFountain L, Caldwell JA. Analysis and design of evapotranspirative cover for hazardous waste landfill. *J Geotech Geoenviron Eng*. 2003;129(5):427–438. [http://dx.doi.org/10.1061/\(asce\)1090-0241\(2003\)129:5\(427\)](http://dx.doi.org/10.1061/(asce)1090-0241(2003)129:5(427)).
21. Zheng S, Xing X, Lourenço SD, Cleall PJ. Cover systems with synthetic water-repellent soils. *Vadose Zone J*. 2021;20(1). <http://dx.doi.org/10.1002/vzj2.20093>.
22. Benson C, Bareither C. Designing water balance covers for sustainable waste containment: Transitioning state-of-the-art to state-of-the-practice by Craig H. Benson 1 and Christopher A. Bareither 2 1. In: Rollins K, Zekkos D, eds. *Geotechnical Engineering State of the Art and Practice*. ASCE; 2012:1–33.
23. Bareither CA, Foley JC, Benson CH. Using surrogate meteorological data to predict the hydrology of a water balance cover. *J Geotech Geoenviron Eng*. 2016;142(4):04015092. [http://dx.doi.org/10.1061/\(asce\)jgt.1943-5606.0001437](http://dx.doi.org/10.1061/(asce)jgt.1943-5606.0001437).
24. Ng CW, Liu J, Chen R, Xu J. Physical and numerical modeling of an inclined three-layer (silt/gravelly sand/clay) capillary barrier cover system under extreme rainfall. *Waste Manag*. 2015;38(1):210–221. <http://dx.doi.org/10.1016/j.wasman.2014.12.013>.
25. Khire MV, Benson CH, Bosscher PJ. Field data from a capillary barrier and model predictions with UNSAT-H. *J Geotech Geoenviron Eng*. 1997;125(6).
26. Elia G, Cotecchia F, Pedone G, Vaunat J, Vardon PJ, Pereira C, Springman SM, Rouainia M, Van Esch J, Koda E, Josifovski J, Nocilla A, Askarinejad A, Stirling R, Helm P, Lollino P, Osinski P. Numerical modelling of slope-vegetation-atmosphere interaction: An overview. *Q J Eng Geol Hydrogeol*. 2017;50(3):249–270. <http://dx.doi.org/10.1144/qjgeh2016-079>.
27. Kovacevic N, Potts DM, Vaughan PR. Progressive failure in clay embankments due to seasonal climate changes. In: *International Conference on Soil Mechanics and Geotechnical Engineering*. Istanbul, Turkey: Balkema; 2001:2127–2130.
28. C. SPG. *Numerical Analysis of Infiltration into Partially Saturated Soil Slopes* (Ph.D. thesis). Imperial College London, University of London; 2003.
29. Smith PG, Potts DM, Addenbrooke TI. A precipitation boundary condition for finite element analysis. In: *Unsaturated Soils: Advances in Geo-Engineering - Proceedings of the 1st European Conference on Unsaturated Soils, E-UNSAT 2008*. 2008:773–778. <http://dx.doi.org/10.1201/9780203884430.ch105>.
30. Tsiampousi A, Zdravkovic L, Potts DM. Soil-atmosphere interaction in unsaturated cut slopes. *E3S Web Conf*. 2016;9. <http://dx.doi.org/10.1051/e3sconf/20160908004>.
31. Tsiampousi A, Zdravkovic L, Potts DM. Numerical study of the effect of soil-atmosphere interaction on the stability and serviceability of cut slopes in London clay. *Can Geotech J*. 2017;54(3):405–418. <http://dx.doi.org/10.1139/cgj-2016-0319>.
32. Rouainia M, Davies O, O’Brien T, Glendinning S. Numerical modelling of climate effects on slope stability. *Proc Inst Civ Eng: Bridge Eng*. 2009;162(2):81–89. <http://dx.doi.org/10.1680/jensu.2009.162.2.81>.
33. Davies O, Rouainia M, Glendinning S, Cash M, Trento V. Investigation of a pore pressure driven slope failure using a coupled hydro-mechanical model. *Eng Geol*. 2014;178(February 2018):70–81. <http://dx.doi.org/10.1016/j.enggeol.2014.05.012>.
34. Rouainia M, Helm P, Davies O, Glendinning S. Deterioration of an infrastructure cutting subjected to climate change. *Acta Geotech*. 2020;15(10):2997–3016. <http://dx.doi.org/10.1007/s11440-020-00965-1>.
35. Potts D, Zdravković L. *Finite Element Analysis in Geotechnical Engineering: Volume One-Theory*. London, UK: Thomas Telford Publishing; 1999.
36. Potts DM, Zdravković L. *Finite Element Analysis in Geotechnical Engineering: Volume Two - Application*. London, UK: Thomas Telford Publishing; 2001.
37. Tsiampousi A, Smith PG, Potts DM. Coupled consolidation in unsaturated soils: An alternative approach to deriving the governing equations. *Comput Geotech*. 2017;84:238–255. <http://dx.doi.org/10.1016/j.compgeo.2016.10.007>.
38. Tsiampousi A, Smith PG, Potts DM. Coupled consolidation in unsaturated soils: From a conceptual model to applications in boundary value problems. *Comput Geotech*. 2017;84:256–277. <http://dx.doi.org/10.1016/j.compgeo.2016.10.008>.
39. Zdravković L, Tsiampousi A, Potts DM. On the modelling of soil-atmosphere interaction in cut and natural slopes. In: *7th International Conference on Unsaturated Soils*. 2018.
40. Tsiampousi A, Zdravković L, Potts DM. Variation with time of the factor of safety of slopes excavated in unsaturated soils. *Comput Geotech*. 2013;48:167–178. <http://dx.doi.org/10.1016/j.compgeo.2012.08.005>.
41. Nyambayo VP, Potts DM. Numerical simulation of evapotranspiration using a root water uptake model. *Comput Geotech*. 2010;37(1–2):175–186. <http://dx.doi.org/10.1016/j.compgeo.2009.08.008>.
42. Feddes RA, Kowalk PJ, Zaradny H. *Simulation of Field Water Use and Crop Yield*. New York: John Wiley and Sons; 1978.
43. Allen GR, Pereira LS, Raes D, Smith M. *FAO Irrigation and Drainage Paper No. 56. Crop Evapotranspiration*. Technical Report; 1998.
44. Kovacevic N, Hight DW, Potts DM. Predicting the stand-up time of temporary London clay slopes at terminal 5, heathrow airport. In: *Stiff Sedimentary Clays: Genesis and Engineering Behaviour - Geotechnique Symposium in Print 2007, Vol. 5*. 2011:241–252. <http://dx.doi.org/10.1680/ssc.41080.0022>.
45. Nyambayo VP. *Numerical Analysis of Evapotranspiration and Its Influence on Embankments* (Ph.D. thesis). Imperial College London; 2003.
46. Indrawan IGB, Rahardjo H, Leong EC. Drying and wetting characteristics of a two-layer soil column. *Can Geotech J*. 2007;44(1):20–32. <http://dx.doi.org/10.1139/T06-090>.
47. Estabragh AR, Javadi AA. Critical state for overconsolidated unsaturated silty soil. *Can Geotech J*. 2008;45(3):408–420. <http://dx.doi.org/10.1139/T07-105>.
48. Tsiampousi A, Zdravkovic L, Potts D. A new hvorslev surface for critical state type unsaturated and saturated constitutive models. *Comput Geotech*. 2013;48:156–166. <http://dx.doi.org/10.1016/j.compgeo.2012.09.010>.
49. Tsiampousi A, Zdravković L, Potts DM. A three-dimensional hysteretic soil-water retention curve. 2013:155–164.
50. Scarfone R, Wheeler SJ, Lloret-Cabot M. A hysteretic hydraulic constitutive model for unsaturated soils and application to capillary barrier systems. *Geomech Energy Environ*. 2020;(100224). <http://dx.doi.org/10.1016/j.gete.2020.100224>.
51. Taboria DM, Potts DM, Zdravković L. On the assessment of energy dissipated through hysteresis in finite element analysis. *Comput Geotech*. 2016;71:180–194. <http://dx.doi.org/10.1016/j.compgeo.2015.09.001>.
52. Kovacevic N, Higgins KG, Potts DM, Vaughan PR. Undrained behaviour of brecciated upper lias clay at empingham dam. *Geotechnique*. 2007;57(2):181–195. <http://dx.doi.org/10.1680/ssc.41080.0024>.
53. Alonso EE, Gens A, Josa A. A constitutive model for partially saturated soils. *Geotechnique*. 1990;40(3):405–430. <http://dx.doi.org/10.1680/geot.1991.41.2.273>.
54. Georgiadis K, Potts DM, Zdravković L. Three-dimensional constitutive model for partially and fully saturated soils. *Geotechnique*. 2005;244(11):2–3. [http://dx.doi.org/10.1061/\(ASCE\)1532-3641\(2005\)5](http://dx.doi.org/10.1061/(ASCE)1532-3641(2005)5).